International Journal of Rotating Machinery, 8(1): 45–56, 2002

1023-621X/02 $12.00 + .00

Application of the Full Cavitation Model to Pumps and Inducers

MAHESH M. ATHAVALE*, H. Y. LI, YU JIANG, and ASHOK K. SINGHAL
CFD Research Corporation, 215 Wynn Dr., Huntsville, Alabama, 35805, USA

A new "full cavitation model" has been recently developed for performance predictions of engineering equipment under cavitating flow conditions. A vapor transport equation is used for the vapor phase and it is coupled with the turbulent N – S equations. The reduced Rayleigh–Plesset equations are used to account for bubble formation and to derive the time-mean phase-change rates utilizing the local pressures and characteristic velocities. Effects of turbulent fluctuations and noncondensable gases are also included to make the model complete. The model has been incorporated into an advanced finite-volume, pressure-based, commercial CFD code (CFD – ACE+) that uses unstructured/hybrid grids to integrate the N – S equations. Full model details are being published separately. Presented here are simulations of cavitating flows in three types of machines: water jet propulsion axial pump, a centrifugal water pump, and an inducer from a LOX turbo pump. The results show cavitation zones on the leading edge-suction side of each of the machines as expected. Simulations at different suction specific speeds were performed for the waterjet pump and the inducer and showed the proper trends of changes in cavity strength and sizes. All the test cases with cavitation show plausible results (no negative pressures, and good convergence characteristics). Computations on the waterjet pump for different noncondensible gas concentrations showed sizeable changes in the pump head developed.

Keywords: Cavitation; Computational fluid dynamics; Rotating machinery; Inducers

Cavitation is usually found in fluid flows where the local pressure drops below the saturation vapor pressure of the liquid, causing liquid evaporation and generation of vapor bubbles in the low pressure region. Fluid machinery is a common application where low pressures are routinely generated by the machine action, e.g., on blade surfaces, with a consequent possibility of cavitation. Other applications where cavitation is present include hydrofoils (Shen, 1989), submerged moving bodies (Kunz, 1999), and automotive fuel injectors, and draft tubes in turbines (Song, 1999).

Existence of cavitation is often undesired, because it can degrade the device performance, produce undesirable noise, lead to physical damage to the device and affect the structural integrity. Details of the existence, extent and effects of cavitation can be of significant help during the design stages of fluid machinery, in order to minimize cavitation or to account for its effects and optimize the designs. Use of computational fluid dynamics (CFD) codes to analyze the viscous, turbulent flows in fluid machinery has become fairly common, and advanced CFD code, together with a robust, validated cavitation model will be of significant use for performance optimization of fluid machinery and devices in presence of cavitation.

Past several decades have seen considerable research on cavitation and extensive reviews are available in the literature (Acosta, 1974; Brennen, 1995; Arndt, 1981; Kueny, 1993). Different aspects of this complex phenomenon have been explored, including, e.g., cavitation bubble collapse (Wang, 1994; Nguyen-Shafer, 1997) and erosion damage (Soyama, 1991), cavitation acoustics (Ceccio, 1991), cloud cavitation (Wang, 1994), and rotating cavitation (Tsujimoto, 1994). Incorporation of cavitation models into multi-dimensional CFD tools has also been under study and applied to different flow problems including sheet cavitation (Merkle, 1998) and cavitation on submerged bodies (Kunz, 1999). The authors and colleagues have been active in development of cavitation models, incorporation into advanced codes and application to different flow devices (Singhal, 1997; Vaidya, 1998).

The current effort is based on the application of the recently developed full cavitation model that utilizes the

Received in final form 5 May 2000.
This work was supported in part under NSF Grant No. DMI-9801239 (Dr. Cynthia Ekstein, Program Manager); this support is gratefully acknowledged. Thanks are due to Dr. N. Vaidya for his help in cavitation model formulation and to Ms. Swann for preparing the manuscript.
*Corresponding author. E-mail: mma@cfdrc.com

modified Rayleigh–Plesset equations for bubble dynamics and includes the effects of turbulent pressure fluctuations and non-condensible gases (ventilated cavitation) to rotating cavitation in different types of fluid turbomachines.

DESCRIPTION OF THE NUMERICAL MODEL

The cavitation model accounts for all first-order effects, i.e., phase change, bubble dynamics, turbulent pressure fluctuations, and non-condensible gases present in the liquid. The phase change rate expressions are derived from the Rayleigh–Plesset equations, and limiting bubble size (interface surface area per unit volume of vapor) considerations. Full derivation, along with model validations, are being presented in a separate paper. Here only the final expressions and pertinent assumptions are summarized.

The vapor transport equation governing the vapor mass fraction, f, is given by:

$$\frac{\partial}{\partial t}(\rho f) + \nabla \cdot (\rho \bar{V} f) = \nabla \cdot (\Gamma \nabla f) + R_e - R_c \qquad [1]$$

where $\bar{V}$ is the velocity vector, Γ is the effective exchange coefficient, and R_e and R_c are the vapor generation and condensation rate terms. The evaporation and condensation rates are functions of the instantaneous, local static pressure and are given by:

(a) when $P < P_{\text{sat}}$:

$$R_e = C_e \frac{V_{\text{ch}}}{\sigma} \rho_{\text{l}} \rho_{\text{v}} \left[\frac{2}{3} \frac{P_{\text{sat}} - P}{\rho_{\text{l}}} \right]^{1/2} (1 - f) \qquad [2]$$

(b) when $P < P_{\text{sat}}$:

$$R_c = C_c \frac{V_{\text{ch}}}{\sigma} \rho_{\text{l}} \rho_{\text{l}} \left[\frac{2}{3} \frac{P - P_{\text{sat}}}{\rho_{\text{l}}} \right]^{1/2} f \qquad [3]$$

where suffixes l and v denote the liquid and vapor phases, V_{ch} is a characteristic velocity, σ is the surface tension of the liquid, P_{sat} is the saturation vapor pressure of the liquid for the given temperature, and C_e and C_c are empirical constants (in the present form these constants have appropriate dimensions to balance Eqs. [2] and [3]).

The above relations are based on the following assumptions:

1. In the bubble flow regime, the interface area per unit volume is equal to $3/R_b$, and the bubble size (R_b) is limited by the balance between the aerodynamic shear force and the surface tension force. This implies that the phase change rate should be proportional to V_{rel}^2/σ. However, in most practical two-phase flow conditions with large number of bubbles, or bubble cloud type of conditions, the dependence on velocity is somewhat weaker and is assumed to be linear rather than quadratic.
2. In the bubble flow regime, the relative velocity between the vapor and liquid phases is of the order of 1 to 10 percent of the mean velocity. In most turbulent flows the local turbulent velocity fluctuations are also of this order. Therefore, as a first pragmatic approximation, square root of local turbulent kinetic energy $\sqrt{k}$ is used for V_{ch} in Eqs. [2] and [3].
3. The preliminary values of the coefficients C_e and C_c are set to 0.02 and 0.01, respectively. These values were arrived at by parametric studies over a wide range of flow conditions in orifice and hydrofoil problems.
4. A constant surface tension value of 0.075 N/m was used for calculations with water.

Further calibration and validation is in progress and the final values will be reported in a separate paper with the full description of the model.

Effects of Turbulent Pressure Fluctuations

Several experimental investigations have shown significant effect of turbulence on cavitating flows (e.g., Keller, 1997). A few years ago, present authors reported a numerical model (Singhal, 1997), using a probability density function (PDF) approach for accounting the effects of turbulent pressure fluctuations. This approach required: (a) estimation of the local values of the turbulent pressure fluctuations as:

$$P'_{\text{turb}} = 0.39 \rho k \qquad [4]$$

and (b) computations of time-averaged phase-change rates ($\bar{R}_e$ and $\bar{R}_c$) by integration of instantaneous rates (R_e and R_c) in conjunction with assumed PDF for pressure variation with time. In the present model, this treatment has been simplified by simply raising the phase-change threshold pressure value from P_{sat} to $(P_{\text{sat}} + P'_{\text{turb}}/2)$.

Effects of Noncondensible Gases

In most engineering equipment, the operating liquid has small finite amount of non-condensible gases present. These can be in dissolved state, or due to leakage, or by aeration. However, even the small amount of (e.g., 10 ppm) of non-condensible gases can have significant effects on the performance of the machinery. The primary effect is due to the expansion of gas at low pressures. This can lead to significant values of local gas volume fraction, and thus have considerable impact on density, velocity and pressure distributions. The working fluid is assumed to be a mixture of the liquid phase and the gaseous phase, with the gaseous phase comprising of the liquid vapor and the noncondensible gas. The density of the mixture, ρ, is variable, and is calculated as

$$\frac{1}{\rho} = \frac{f_v}{\rho_v} + \frac{f_g}{\rho_g} + \frac{1 - f_v - f_g}{\rho_l} \qquad [5]$$

where ρ_l is the liquid density, and ρ_v and ρ_g are the vapor and noncondensible gas densities, respectively, and f_l, f_v and f_g are the mass fractions of the liquid phase, vapor phase and noncondensible gas. The volume fractions of the individual components can be calculated from the mass fractions as, e.g.,

$$\alpha_v = f_v \frac{\rho}{\rho_v}. \qquad [6]$$

The secondary effect of the non-condensible gases can be on the inception of cavitation by increasing the number of nucleation sites for bubble formation. This can be included as a refinement in the empirical coefficients (C_e and C_c), perhaps as a functional dependence on f_g. This is planned to be investigated later.

COMPUTATIONAL RESULTS AND DISCUSSION

The full cavitation model has been implemented in an advanced, general purpose, commercial CFD code, CFD–ACE+. It was applied to a number of rotating cavitation problems encountered in turbomachines to assess its robustness and capability of predicting the occurrence, extent and strength of cavitation zones. Cavitation, when present, typically alters the pressure field on the working surfaces of the turbomachine, with two obvious effects. Changes in blade pressure will alter the amount of work being put into the fluid, which changes the machine performance. Cavitation also will change the blade loading and have impact on the mechanical design of the blades.

Three different applications of turbomachines are presented here: an axial pump, a centrifugal pump and a rocket inducer. Each of the applications presents a different set of conditions and serves to illustrate the usability of the cavitation model. Given below are details of the flow simulations.

Axial Pump

The pump considered operates in a waterjet propulsion system used on marine ships (e.g., see Allison, 1993). It has two stages: an inducer with four blades and an impeller (kicker) with eight blades mounted on a single shaft. The pump operates at a near-constant flow rate and speed. The static pressure at the inlet depends on the ship speed, and can vary between 0.1 to 1 bar. This can lead to cavitation on the inducer blades over a large portion of the operating envelope. In the extreme cavitation case the entire inducer blade could be covered with cavitation with minimal zones on the impeller blades.

The computational model used one blade-to-blade passage of the inducer and 2 passages of the impeller to maintain periodicity. A single-domain structured grid was generated with approx. 65000 cells. Both the inducer and

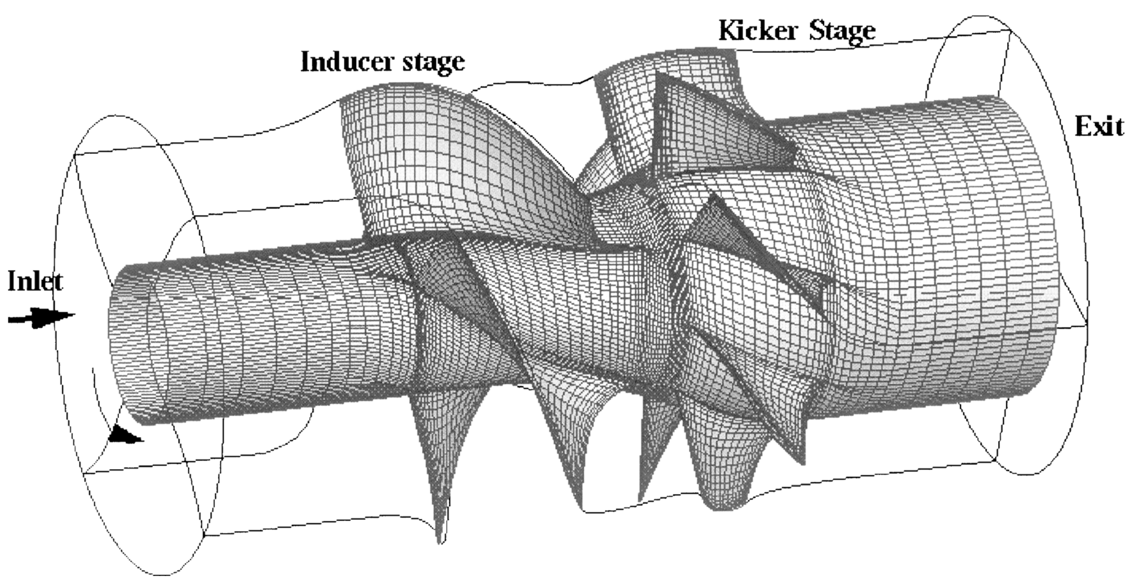

FIGURE 1 Solids model of the axial waterjet pump with flow and boundary condition.

impeller blades have tip gaps and 3 cells were used in the gap region. Working fluid was water at 290 K, with a liquid-to-vapor density ratio of about 70000. Turbulence in the flow was handled using standard k–ε model with wall functions. Appropriate stationary or rotating wall conditions were imposed on solid surfaces. Inlet boundary was a specified flow rate with a static pressure condition at the outlet. The exit static pressure was adjusted during computations to produce the desired inlet static pressure levels. A very small noncondensible air fraction of 0.5 ppm was used. Figure 1 shows the computational grid and boundary conditions.

RESULTS

Flow simulations at three different suction specific speed (Nss) values (US standard) were considered which covered nearly the entire range of Nss likely to be encountered. The specific values were approximately 13400, 15800, and 19200. In each case the solution was considered converged after a minimum residual drop of 4 orders of magnitude. In all the cases this required less than 900 iterations. A sample convergence plot is shown in Figure 2. Figure 3A shows the single-phase pressure field for Nss = 19200 with the negative pressure areas on the suction side of the inducer blades. The cavitating flow solutions of the pressure field are shown in Figure 3B. Cavitation zone extent can be estimated using the void fraction plots and the surface distribution is shown in Figure 4A. (The value of the volume fraction that signifies the apparent boundaries of the cavitation zone is rather arbitrary and the practice adopted here is to use a value that is slightly higher than the non-condensible gas fraction; the typical values used here are a volume fraction of 0.0001 or so). In the present case the cavitation zone extends over the entire suction side of the inducer blade. The calculations also predict a fair amount of cavitation on the kicker blade leading edge. Reduction in Nss in present case indicates a higher upstream pressure, and hence represents less favorable conditions for *cavitation*, Figure 4B shows the void fraction plot for Nss = 15800. For this case a triangular-shaped cavitation zone, occupying perhaps 40% of the leading portion of blade suction side is seen. Effects of cavitation on blade pressure profiles are of importance for mechanical design, and a representative pressure plot along the blade

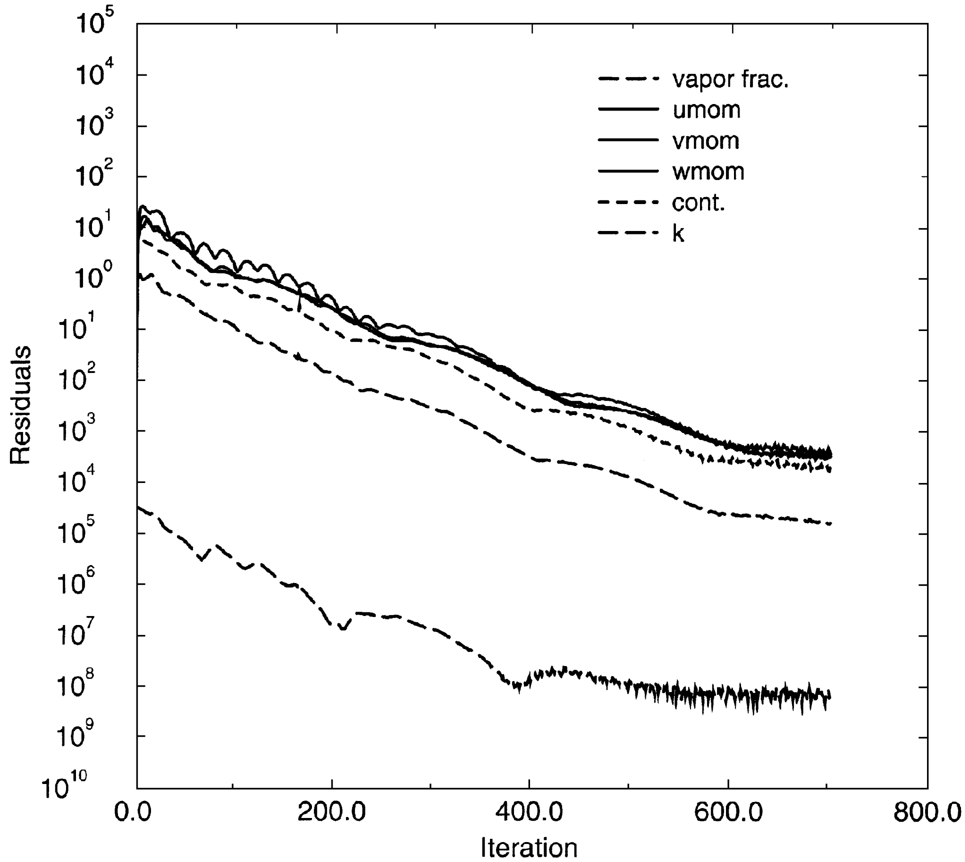

FIGURE 2 Sample convergence plot for the cavitation run on the axial waterjet pump (See Colour Plate at back of issue.).

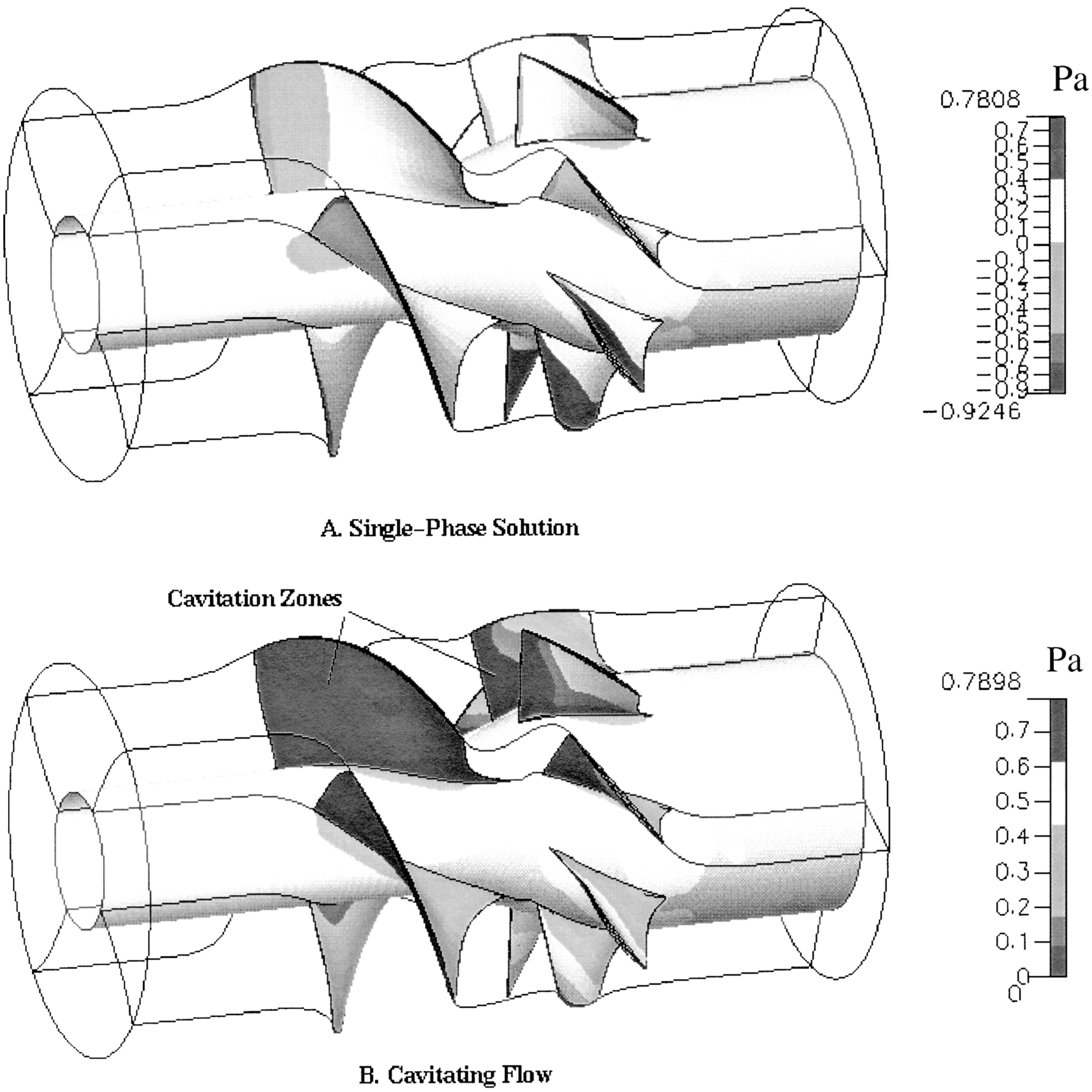

FIGURE 3 Normalized static pressure field in the waterjet pump for Nss = 19000 (See Colour Plate at back of issue.).

chord length near the suction side tip is shown in Figure 5 where the single-phase and cavitation solutions are plotted. The pressure in the cavitation zone is nearly constant and positive, compared to the negative pressure zone in the single-phase solution.

For a marine application the presence of non-condensing gas can be expected to affect the cavitation characteristics and the pump performance, and this was explored to some extent by conducting another simulation at Nss = 19200, where the noncondensible air fraction was increased to 5 ppm. The corresponding pressure field is plotted in Figure 6. The calculated pump head rise for this case showed a decrease of about 4.5% from the earlier calculation with 0.5 ppm air concentration. Further investigations of this effect are in progress.

Centrifugal Water Pump

This is a common design used for pumping water with a moderate head increase. For a given flow rate, the inlet conditions depend on the height difference between the inlet plane and the lower reservoir. If this difference is large, the inlet static pressure can become low enough to produce cavitation on the leading portion of the blades. In the present simulation, the inlet pressure level corresponds to a Nss of approximately 6200.

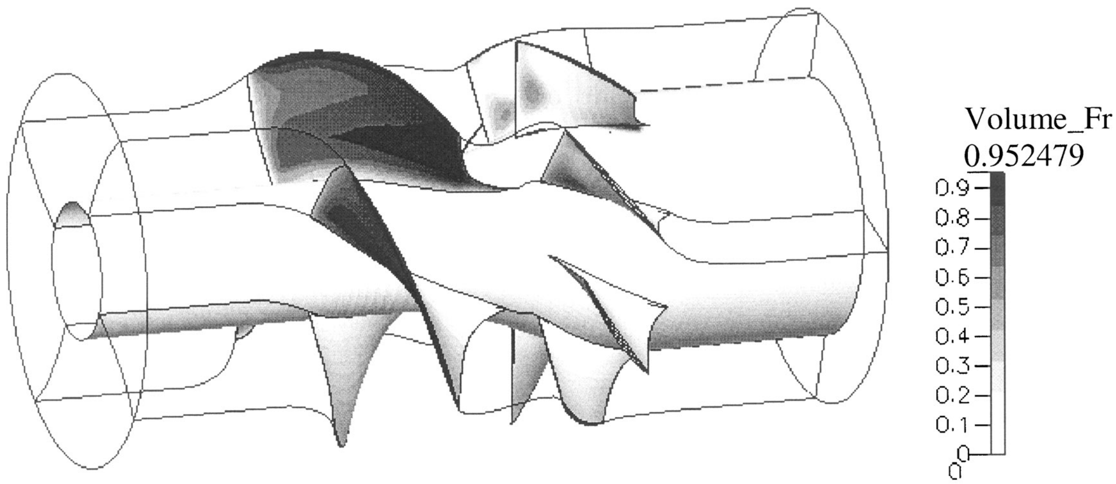

A. Nss = 19,000, Entire Suction Side Shows Cavitation

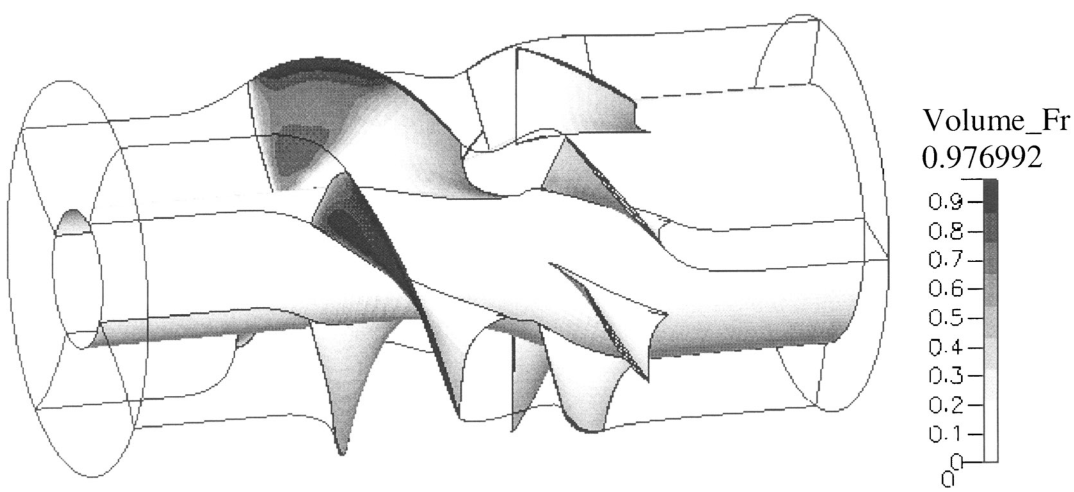

B. Nss = 15,800, Smaller Triangle-Shaped Cavitation Near Leading Edge

FIGURE 4 Vapor volume fraction on solid surfaces, indicating the extent of cavitation for two different Nss values.

A 2-domain, structured grid with 53000 cells was generated for this 6 bladed pump, with a single blade-to-blade passage as the working domain. A constant inlet axial velocity was specified at the inlet plane. A vaneless diffuser section was used after the impeller blade exit. Figure 7 shows the computational model of this pump. Working fluid was water at 290 K. Standard k–ε turbulence model was used for the turbulent flow. The non-condensible gas fraction was set to 0.5 ppm.

RESULTS

The computed static pressure field for cavitating flow is shown in Figure 8. The predicted cavitation zone is located in the leading portion of the suction side as shown by the volume fraction plotted on the solid surfaces, shown in Figure 9. The severity and extent of this case is relatively low and a only a small decrease in the head developed was seen for this particular case.

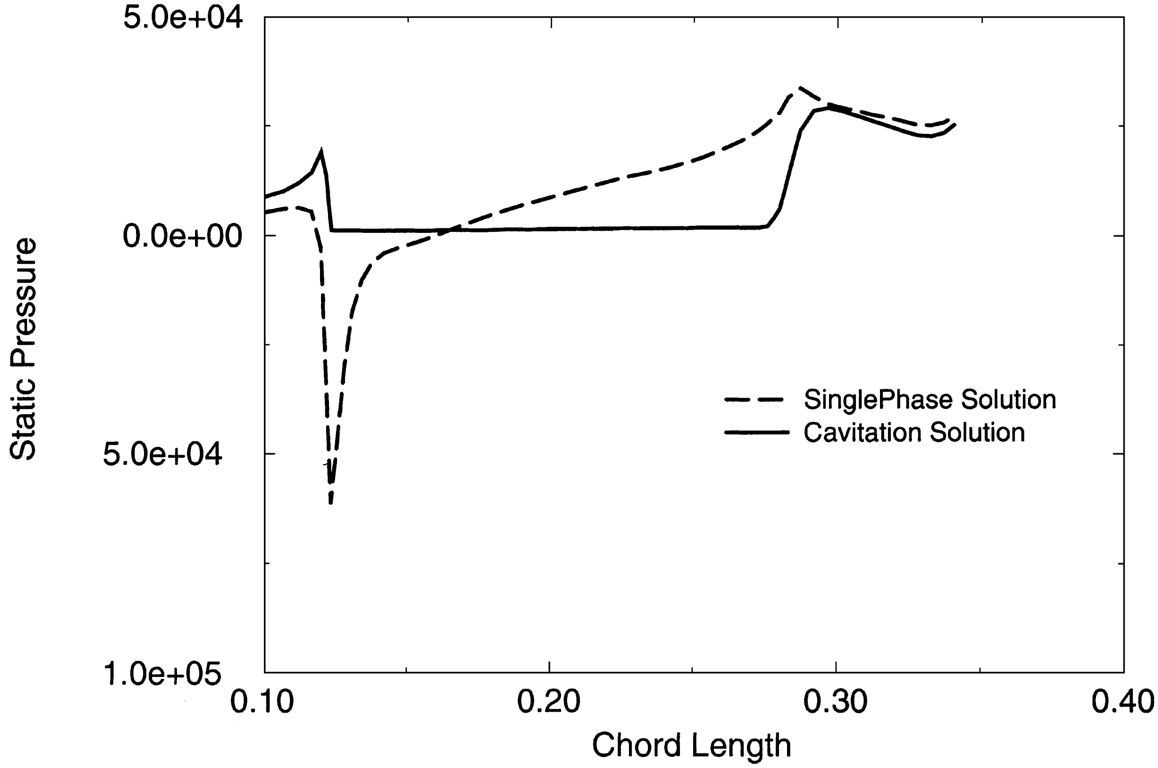

FIGURE 5 Pressure profile on the suction side tip region of the inducer stage of waterjet pump. Cavitation solution at Nss = 19200.

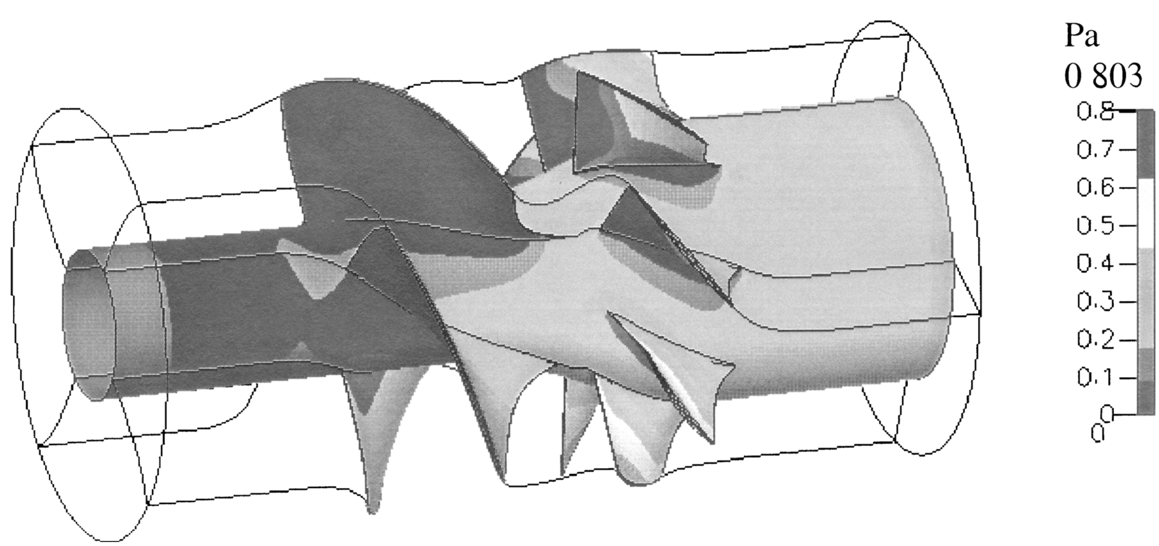

FIGURE 6 Static pressure distribution in the pump for an air concentration of 5 ppm. Compare with results from Figure 3B (See Colour Plate at back of issue.).

Liquid Oxygen Rocket Inducer

This application is from a high-performance liquid oxygen pump used in a rocket engine. The pump consists of an induce followed by a centrifugal impeller. The inducer operates in a regime where cavitation is expected. The pressurization in the inducer is relatively high, and this eliminates the possibility of cavitation in the impeller. The inducer has 4 blades, with a blade angle of approx. 76 degrees with the rotational axis. The rotational speed is

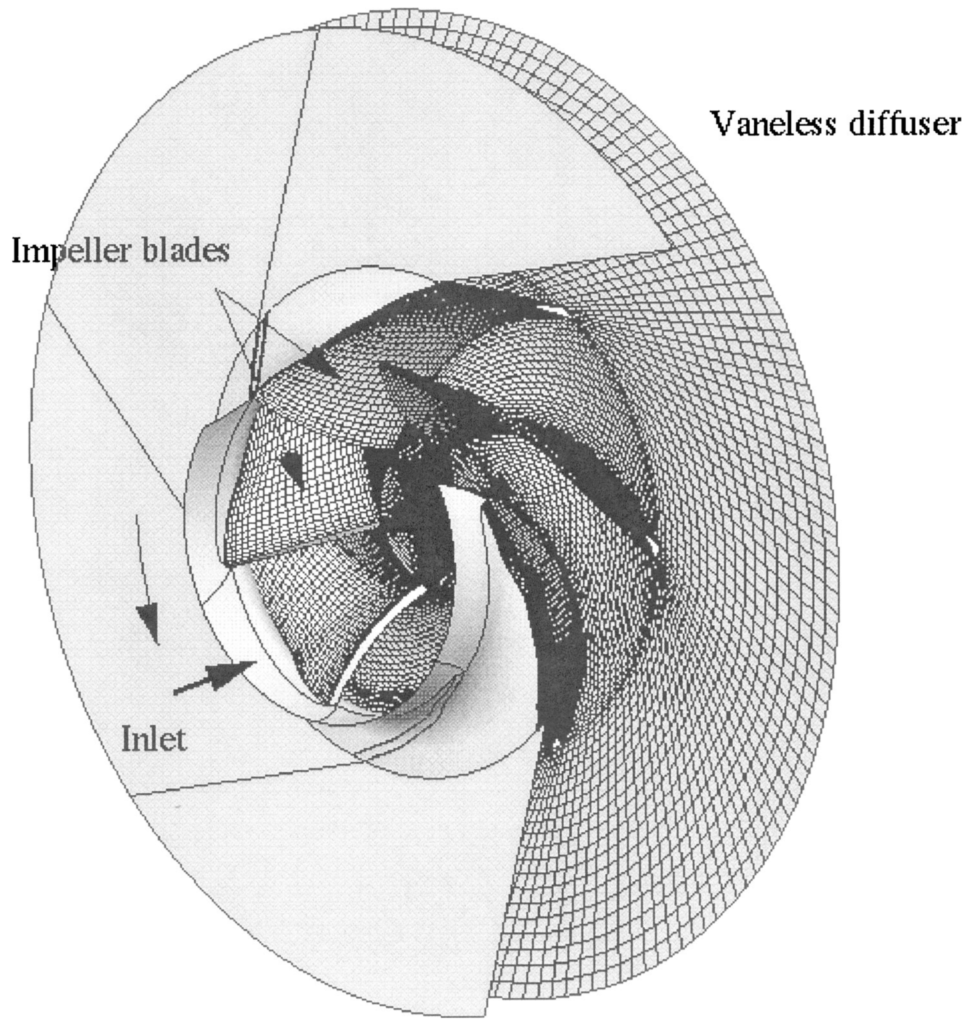

FIGURE 7 Computational grid and model of the centrifugal water pump.

23000 rpm. The operating conditions yield an Nss of approx. 15000. Cavitation occurs near the initial portion of the blade suction surface near the tip. The extent of the cavitation in axial direction is relatively small because of rapid pressurization.

A single domain grid with approx. 43000 cells was generated for this geometry, with blocked cells representing the blade (Figure 10). A mass flux at the inlet boundary was specified, with a specified static pressure at the exit boundary. The standard $k-\varepsilon$ turbulence model was used. As in the previous cases, the single phase solutions yielded pressurization across the inducer, and then the exit static pressures were adjusted to yield the required inlet pressure levels. Solutions at three Nss values of 9000, 13000, and 15000 were obtained to evaluate the changes in the cavitation zone.

RESULTS

Results from the Nss = 15000 case are presented in Figures 11 and 12. The surface pressures for the cavitating flow are shown in Figure 11 and, as before, all positive. The predicted cavitation zones are approximately near the leading edge suction side of the blade, as shown by the cavitation bubble boundaries, shown in Figure 12A. As seen here, the LOX vapor zone extends out to nearly the mid passage away from the blade. When Nss was lowered to 13000, i.e., the upstream pressure levels were increased, the cavitation bubble became much smaller as shown in Figure 12B. Sample line plots of the blade pressure distributions on the suction side tip region are shown in Figure 13 for the single phase and cavitating flow and clearly show the influence of cavitation, where a fair

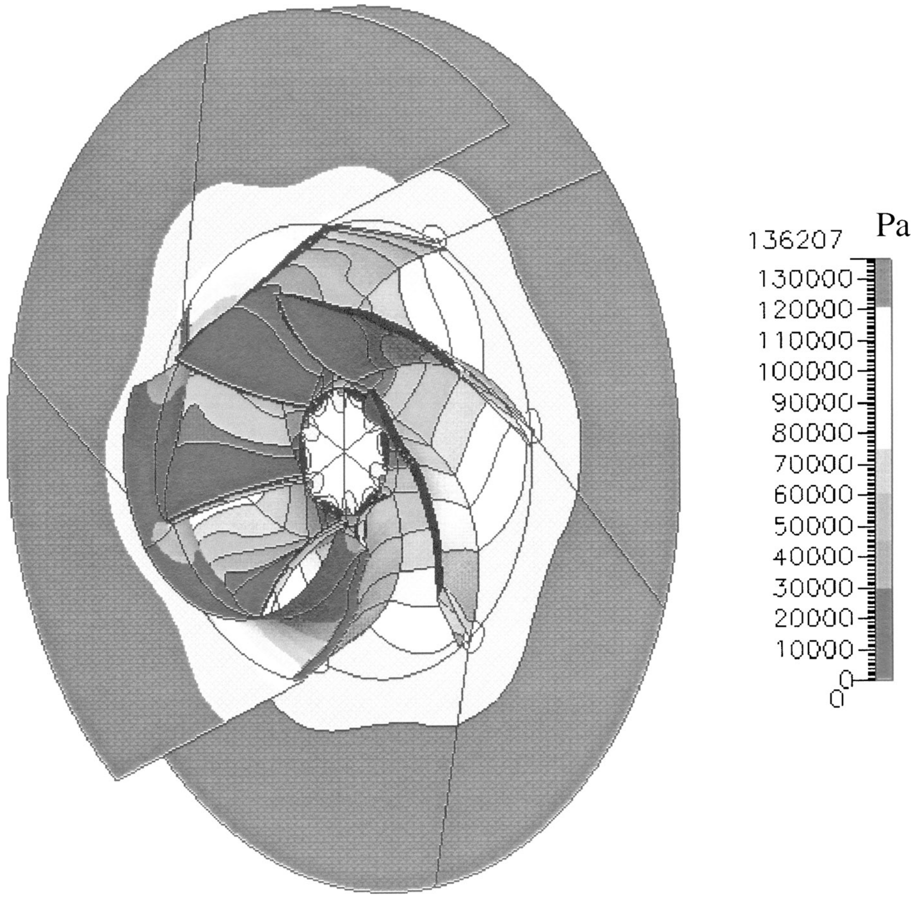

FIGURE 8 Surface pressure field for the centrifugal pump, cavitating flow (See Colour Plate at back of issue.).

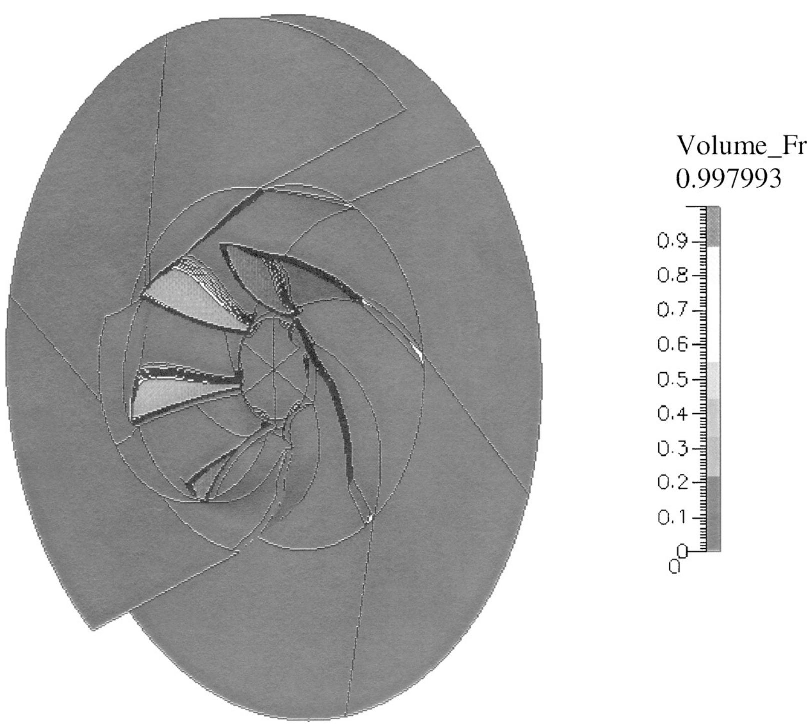

FIGURE 9 Void fraction distribution, showing the cavitation zone and extent, centrifugal pump, $Nss = 6200$ (See Colour Plate at back of issue.).

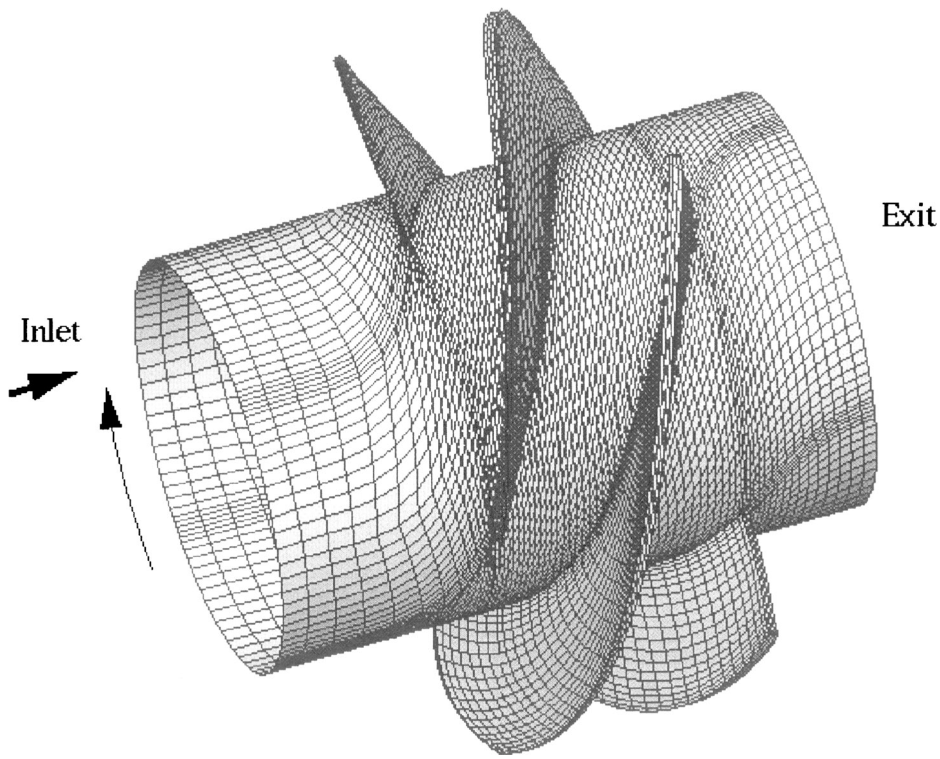

FIGURE 10 Computational model of the rocket inducer.

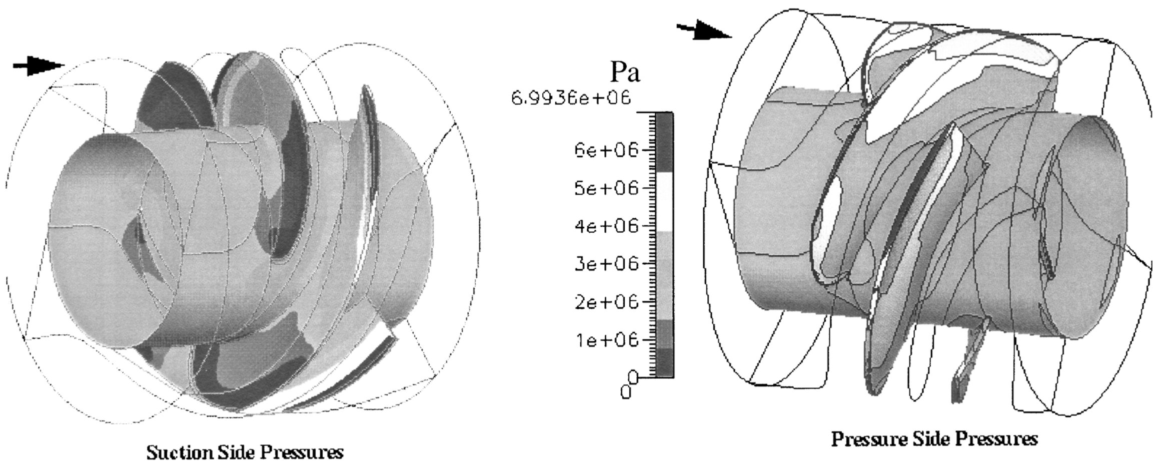

FIGURE 11 Static pressures on solid surfaces for the inducer, cavitating flow, Nss = 15000 (See Colour Plate at back of issue.).

amount of pressure redistribution on the blade surface behind the cavitation zone is seen.

SUMMARY AND CONCLUSIONS

The full cavitation model has been applied to cavitating flows in three different turbomachine elements, namely a two-stage axial pump, centrifugal water pump, and a high-performance rocket pump inducer. The three examples offered different challenges to the flow solver in terms of either severity of operating conditions (rocket inducer) or very high density ratios (water) in the other two problems. In each case, the model predictions were physically plausible, and the numerical convergence behavior was very robust and stable. The simulation results predict several of the

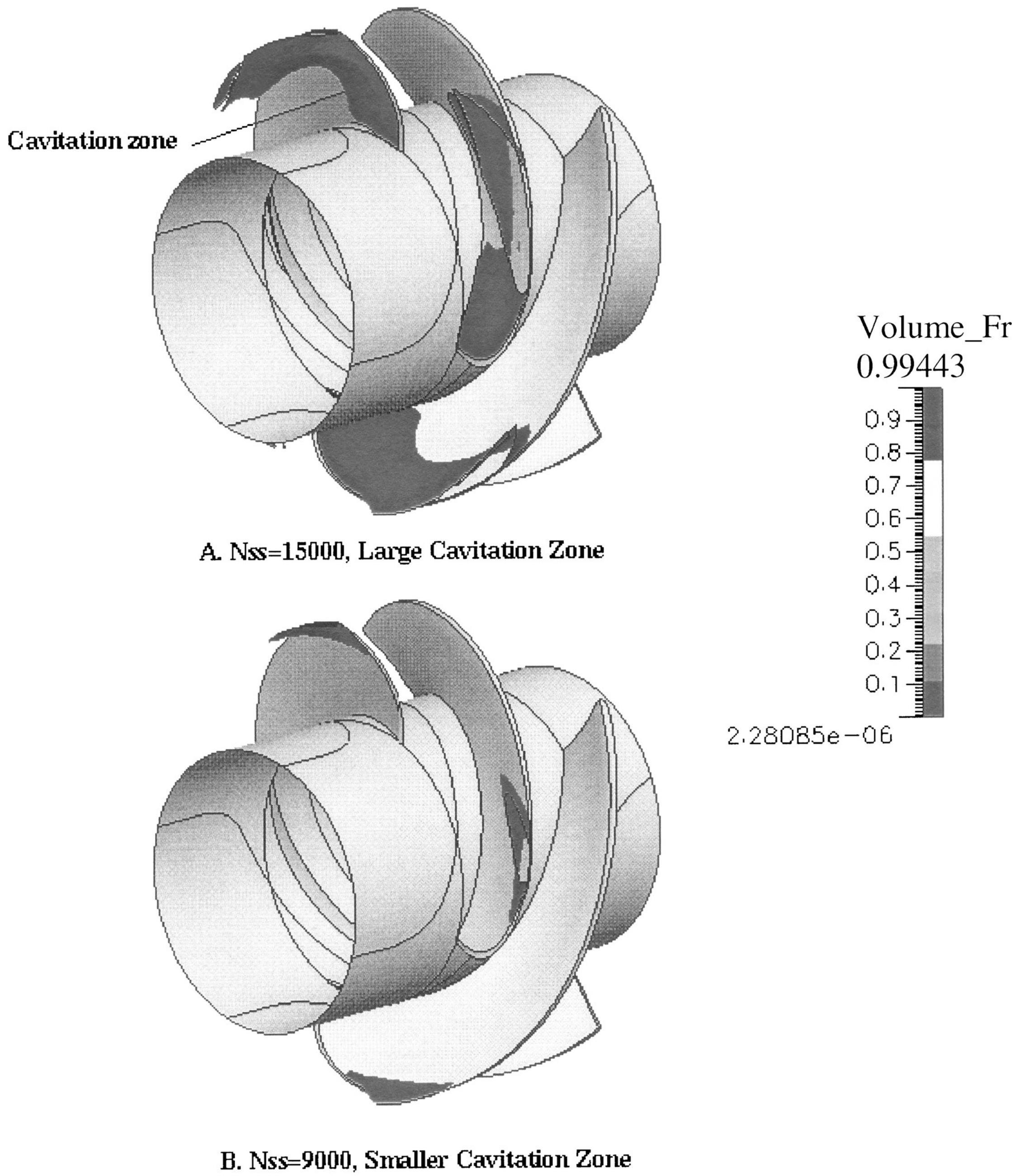

FIGURE 12 Extent of the cavitation zone in the inducer at different Nss values (See Colour Plate at back of issue.).

anticipated trends correctly, namely variation of size, location and shape of cavitation zone with different Nss values. In all of the cases, the cavitating flows showed positive pressure levels at all places in the cavitation zones. The effects of the noncondensible gases on cavitation and pump performance were explored for the waterjet pump. Initial tests show that the presence of noncondensible gases reduced the pump head as well as the extent of the cavitation zone. This aspect will be of importance in a variety of applications and needs further work. Further development is needed for better calibration of the coefficients C_e and C_c. If necessary these can also be made functions of physical effects such as water quality (f), surface roughness, *etc.* Additional, more through validation work on the full cavitation model, and applications to other problems is in progress and will be reported separately.

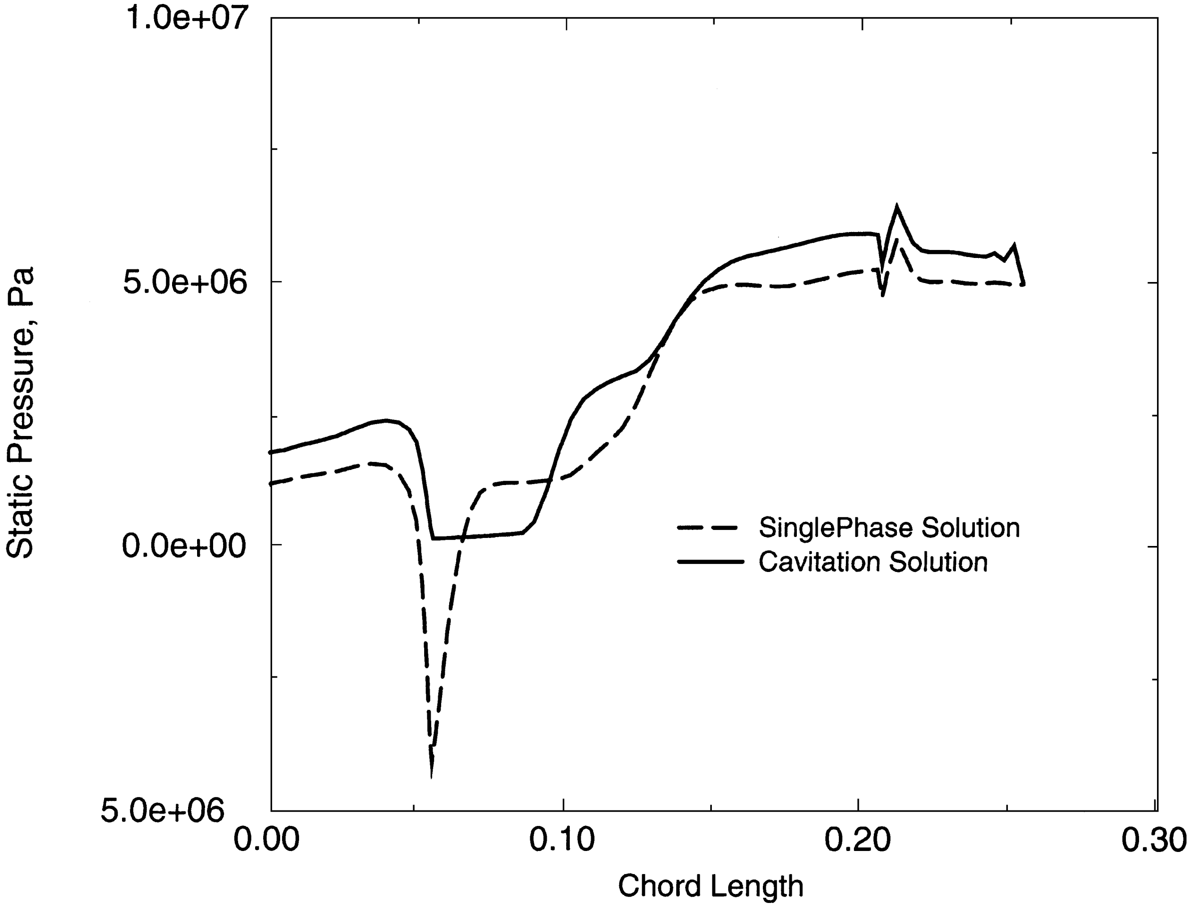

FIGURE 13 Pressure profile on the suction side tip region of LOX inducer, Nss = 15000.

REFERENCES

Acosta, A. J. (1974) Cavitation and Fluid Machinery, *Proc. of Cavitation Conference*, Heriot-Watt Univ. of Edinburgh, Scotland, pp. 383–396.

Allison, J. L. (1993) Marine Waterjet Propulsion, *Trans. Soc. of Naval Architects and Marine Engineers*, **101**, 275–335.

Arndt, R. E. A. (1981) Cavitation in Fluid Machinery and Hydraulic Structures, *Ann. Rev. of Fluid Mech.*, **13**, 273–328.

Brennen, C. E. (1995) *Cavitation and Bubble Dynamics*, Oxford University Press.

Ceccio, S. L. and Brennen, C. E. (1991) Observations of the Dynamics and Acoustics of Traveling Bubble Cavitation, *J. Fluid Mechanics*, **223**, 633–660.

Keller, A. P. and Rott, H. K. (1997) The Effect of Flow Turbulence on Cavitation Inception, Munich University of *Tech. Report*, *ASME-FED Meeting*, Vancouver, Canada.

Kueny, J. L. (1993) *Cavitation Modeling*, *Lecture Series*: *Spacecraft Propulsion*, Von Karman Institute for Fluid Dynamics.

Kunz, R. F., Boger, D. A., Chyczewski, T. S., Stineberg, D. R., Gibeling, H. J. and Govindan, T. R. (1999) Multi-Phase CFD Analysis of Natural and Ventilated Cavitation About Submerged Bodies, *Proceedings of ASMEN FEDSM-99*.

Merkle, C. L., Feng, J. and Buelow (1998) P.E.O. Computational Modeling of the Dynamics of Sheet Cavitation, *3rd International Symposium on Cavitation*, Grenoble, France.

Nguyen-Schafer, H. and Sprafke, P. (1997) Numerical Study on Interaction Effects of the Bubbles Induced by Air-Release and Cavitation in Hydraulic Systems, *10th Bath International Fluid Power Workshop*, Bath, UK.

Shen, Y. T. and Dimotakis, P. E. (1989) The Influence of Surface Cavitation on Hydrodynamic Forces, *Proc. 22nd ATTC*, St. Johns.

Singhal, A. K., Vaidya, N. and Leonard, A. D. (1997) *Multi-Dimensional Simulation of Cavitating Flows using a PDF Model for Phase Change*, ASME FEDSM97–3272.

Song, C. S., Chen, X., Tani, K., Shinmei, K., Nikura, K. and Sato, J. (1999) *Simulation of Cavitating Flows in Francis Turbine and Draft Tube under OH-Design Conditions*, ASME-FEDSM99-6849.

Soyama, H., Ito, Y., Ichioka, T. and Oba, R. (1991) *SEM Observations of Rapid Cavitation Erosion Arising in a Typical Centrifugal Pump*, ASME FED., Vol. 10.

Tsujimoto, Y., Kamijo, K., Watanabe, S. and Yoshida, Y. (1994) A Non-Linear Calculation of Rotating Cavitation in Inducers, ASME FED., **194**, 53–58.

Vaidya, N., Athavale, M. M. and Singhal, A. K. (1998) Numerical Simulation of Cavitating Flows in an Axial Pump Using a PDF-Based Cavitation Model, ISROMAC-7, Honolulu, Hawaii.

Wang, Y. C. and Brennen, C. E. (1994) Shock Wave Development in the Collapse of a Cloud of Bubbles, ASME-FED., **194**, 15–19.